Structure, Vol. 13, 1269–1277, September, 2005, ©2005 Elsevier Ltd All rights reserved. DOI 10.1016/j.str.2005.06.011

Crystal Structure of IRF-3 in Complex with CBP

Bin Y. Qin,[1] Cheng Liu,[2] Hema Srinath,[1] Suvana S. Lam,[1] John J. Correia,[3] Rik Derynck,[2] and Kai Lin[1,*]

[1]Department of Biochemistry and Molecular Pharmacology
University of Massachusetts Medical School
Worcester, Massachusetts 01605

[2]Department of Cell and Tissue Biology and Department of Anatomy
Programs in Cell Biology and Developmental Biology
University of California, San Francisco
San Francisco, California 94143

[3]Department of Biochemistry
University of Mississippi Medical Center
Jackson, Mississippi 39216

Summary

Transcriptional activation of interferon β (IFN-β), an antiviral cytokine, requires the assembly of IRF-3 and CBP/p300 at the promoter region of the IFN-β gene. The crystal structure of IRF-3 in complex with CBP reveals that CBP interacts with a hydrophobic surface on IRF-3, which in latent IRF-3 is covered by its autoinhibitory elements. This structural organization suggests that virus-induced phosphoactivation of IRF-3 triggers unfolding of the autoinhibitory elements and exposes the same hydrophobic surface for CBP interaction. The structure also reveals that the interacting CBP segment can exist in drastically different conformations, depending on the identity of the associating transcription cofactor. The finding suggests a possible regulatory mechanism in CBP/p300, by which the interacting transcription factor can specify the coactivator's conformation and influence the transcriptional outcome.

Introduction

A key event in mounting the mammalian innate immune response upon virus infection is the transcriptional activation of the antiviral cytokine, interferon β (IFN-β) (Barnes et al., 2002; Maniatis et al., 1998; Taniguchi et al., 2001; Taniguchi and Takaoka, 2002). The pathway leading to IFN-β expression is guarded by IRF-3, a member of the interferon regulatory factor (IRF) family of transcription factors (Hiscott et al., 1999; Servant et al., 2002; Yoneyama et al., 2002). In the absence of virus, IRF-3 is localized in the cytoplasm in a latent form. Virus infection induces IRF-3 phosphorylation and translocation into the nucleus, where it forms a nucleoprotein complex with the closely related coactivators CREB binding protein (CBP) or p300 at the promoter region of the IFN-β gene to activate transcription (Lin et al., 1998; Parekh and Maniatis, 1999; Wathelet et al., 1998; Weaver et al., 1998; Yoneyama et al., 1998).

*Correspondence: kai.lin@umassmed.edu

IRF-3 consists of an N-terminal DNA binding domain and a C-terminal IRF association domain (IAD). The IAD mediates phosphorylation-dependent homooligomerization and heterooligomerization with other IRF members and interacts with CBP/p300. A functional analysis of IRF-3 revealed an autoinhibitory mechanism, mediated by the combined action of sequences flanking the IAD (Lin et al., 1999). The virus-induced phosphoactivation of IRF-3, thought to be mediated by IKKε and/or TBK1, occurs at Ser/Thr sites located C-terminal of the IAD (Fitzgerald et al., 2003; Lin et al., 1998; Sharma et al., 2003; Yoneyama et al., 1998). Virus-induced phosphorylation consequently triggers IRF-3 oligomerization, nuclear translocation, and interaction with CBP/p300 to activate IFN-β expression. Consistent with the results from functional studies, the crystal structure of latent IRF-3 defines a network of intramolecular interactions between N- and C-terminally flanking autoinhibitory elements, which together cover a hydrophobic surface on the IAD (Qin et al., 2003). The structure suggests that phosphorylation results in unfolding of the autoinhibitory structures, thereby opening the hydrophobic surface for functional interactions. A parallel structural study (Takahasi et al., 2003) opposed the existence of an autoinhibitory mechanism and suggested that the phosphorylated residues of IRF-3 directly participate in subunit-subunit contacts within an active dimer without disturbing the structure. The same study also suggested that CBP/p300 interacts with a large acidic surface on IRF-3, formed as a result of subunit dimerization.

The closely related CBP and p300 are general transcriptional coactivators that differentially and combinatorially interact with various transcription factors and comodulators to activate gene expression (Blobel, 2002; Chan and La Thangue, 2001; Goodman and Smolik, 2000; Janknecht and Hunter, 1996). The numerous protein-protein interaction domains in CBP/p300 are all capable of recognizing multiple transcription factors with no apparent sequence or structural similarities. Activation of a specific gene depends on the formation of a nucleoprotein complex between CBP/p300 and a select set of transcription factors at the promoter region of the target gene. The coactivator function of CBP/p300 also depends on its intrinsic acetyltansferase activity and interaction with other acetyltransferases. Acetylation of histones and transcription factors leads to chromatin relaxation and transcript factor activation.

The IRF-3 binding domain (IBiD) of CBP/p300 has been mapped to a 46 residue segment within the C-terminal glutamine-rich region (Lin et al., 2001a). The IBiD can also interact with several other comodulators, such as Ets-2, the adenoviral oncoprotein E1A, the nuclear receptor coactivator protein ACTR, an IRF homolog encoded by the Kaposi's sarcoma-associated herpesvirus, and p53 (Lin et al., 2001a, 2001b; Livengood et al., 2002; Matsuda et al., 2004). The NMR structures of the uncomplexed IBiD and a complex between the IBiD and ACTR have been determined (Demarest et al.,

2002; Lin et al., 2001a). Both structures reveal a helical framework of the IBiD. However, the conformations of the IBiD in the two structures are different, suggesting that the IBiD undergoes a conformational transition upon interaction with a comodulator. The structural basis for the versatility of the IBiD in comodulator interactions is not known.

Here, we report the crystal structure of a complex between the IBiD of CBP and the IAD of IRF-3 at 2.4 Å resolution. The structure reveals that the IBiD binds to a hydrophobic surface on IAD, which in latent IRF-3 is buried by the autoinhibitory elements. The structure further reveals a novel, to our knowledge, conformation of the IBiD that is markedly different from that of the free IBiD or the IBiD in the ACTR/IBiD complex. The result suggests a possible regulatory mechanism in CBP/p300, by which binding of a transcriptional comodulator at the IBiD can stabilize CBP/p300 in one of its multiple conformations to influence the transcriptional outcome.

Results

Overall Structure of the IRF-3/IBiD Complex

The C-terminal transactivation domain of IRF-3 consists of a central IAD flanked on both sides by autoinhibitory sequences (Lin et al., 1999; Qin et al., 2003). To form a stable complex between IRF-3 and the IBiD, it was necessary to use an IRF-3 construct, IRF-3(173-394), without the C-terminal autoinhibitory sequence (data not shown). The crystal structure contains two copies of the IRF-3/IBiD complex in the asymmetric unit (Table 1). The two copies are related by a 2-fold axis, and they have essentially the same structure with a root mean square deviation of 0.1 Å, when superimposed over all atoms. Only one complex is described here since there is no evidence that the interactions between the two copies are physiologically relevant. Analytical ultracentrifugation analysis shows that the exact IRF-3/IBiD complex used in the structural study does not oligomerize in solution (Figure 1A and Figures S1 and S2; see the Supplemental Data available with this article online).

The IAD segment of IRF-3 and the IBiD segment of CBP form a 1:1 complex through interactions primarily between α helices (Figure 1B). The structure of IRF-3 consists of a β sandwich core capped by α helices and loops. Helices H3 and H4 of IRF-3, located on one end of the structural core, form the major interaction surface for the IBiD. The IBiD consists of three α helices (H1, H2, and H3) and a loop (L1), forming an approximately rectangular framework, which interacts with IRF-3 via a flat surface. In the crystal structure of latent IRF-3, the H3 and H4 helices are covered by concerted intramolecular interactions of the autoinhibitory elements, consisting of the N-terminal H1 helix and the C-terminal β12-L6-β13-H5 structure (Figure 1C) (Qin et al., 2003). In the IRF-3/IBiD complex, the IBiD covers the same surface as the autoinhibitory elements in the latent IRF-3 structure (compare Figures 1B and 1C). These observations indicate that the autoinhibitory conformation of latent IRF-3 and the interaction of IRF-3 with the IBiD are mutually exclusive.

Table 1. Summary of Crystal Analysis for the IRF3/IBiD Complex

Parameter	IRF-3/IBiD
Crystal Parameters and Crystallographic Data	
Space group	P6(1)
Unit cell dimensions	a = b = 81.7, c = 242.1
Diffraction limit (Å)[a]	2.37 (2.41–2.37)
Total reflections	122,107
Unique reflections	35,879
Completeness (%)	96.0 (98.4)
Intensity/σ	14.4 (2.0)
R_{merge} (%)[b]	7.8 (44.7)
Refinement Statistics	
Protein atoms	3,720
Water molecules	418
R factor (%)[c]	21.5
R_{free} (%)[d]	22.6
Rmsd from ideal	
Bond (Å)	0.007
Bond (°)	1.3
Ramachandran	
Core (%)	89.1
Allow (%)	10.9
B factor average (Å^2)	
Chain A (IRF-3)	63.6
Chain B (IRF-3)	63.5
Chain C (the IBiD)	69.0
Chain D (the IBiD)	68.7

[a] Values in brackets are for the highest-resolution shell.
[b] $R_{merge} = \Sigma |I_{hkl} - \langle I_{hkl} \rangle| / \Sigma I_{hkl}$.
[c] R factor = $\Sigma_{hkl} ||F_{obs}| - |F_{calc}|| / \Sigma_{hkl} |F_{obs}|$ for all data.
[d] $R_{free} = \Sigma_{hkl} ||F_{obs}| - |F_{calc}|| / \Sigma_{hkl} |F_{obs}|$ for 10% of the data not used in refinement.

The IRF-3/IBiD Interface

The association between IRF-3 and the IBiD covers a hydrophobic interface of approximately 1800 Å^2. The interacting hydrophobic residues of IRF-3 involve primarily Ile326, Leu329, and Ile330 in the H3 helix, as well as Cys371, Leu372, Leu375, Met378, and Val381 in the H4 helix (Figure 1D, right). In addition, Trp202 on the β1 strand also contributes to the buried hydrophobic interface. The interacting hydrophobic residues of the IBiD are distributed over three helices, involving primarily Leu2071 and Leu2075 in the H1 helix; Val2087, Ile2090, and Leu2091in the H2 helix; as well as Leu2097 and Phe2101 in the H3 helix (Figure 1D, left). In addition to these core hydrophobic contacts, the complex is also stabilized by a limited set of H bond interactions on the outskirts of the interface (Figure 1D). The Glu203 side chain of IRF-3 forms an H bond with the Ser2080 side chain of CBP, and the Ser221 side chain of IRF-3 forms an H bond with the Gln2086 side chain of CBP. The Glu201 side chain of IRF-3, although not involved in H bonding interactions, forms a nice van der Waals contact with the Gln2086 side chain of CBP.

To verify that the peptide conformation of the IBiD observed in the crystal structure corresponds to its interaction with IRF-3 in vivo, we performed coimmunoprecipitations of endogenous CBP with ectopically expressed full-length wild-type or mutant IRF-3 in the absence or presence of Sendai viral infection (Figure 2A). Virus infection results in IRF-3 activation and consequent stabilization of the IRF-3/CBP interaction. The

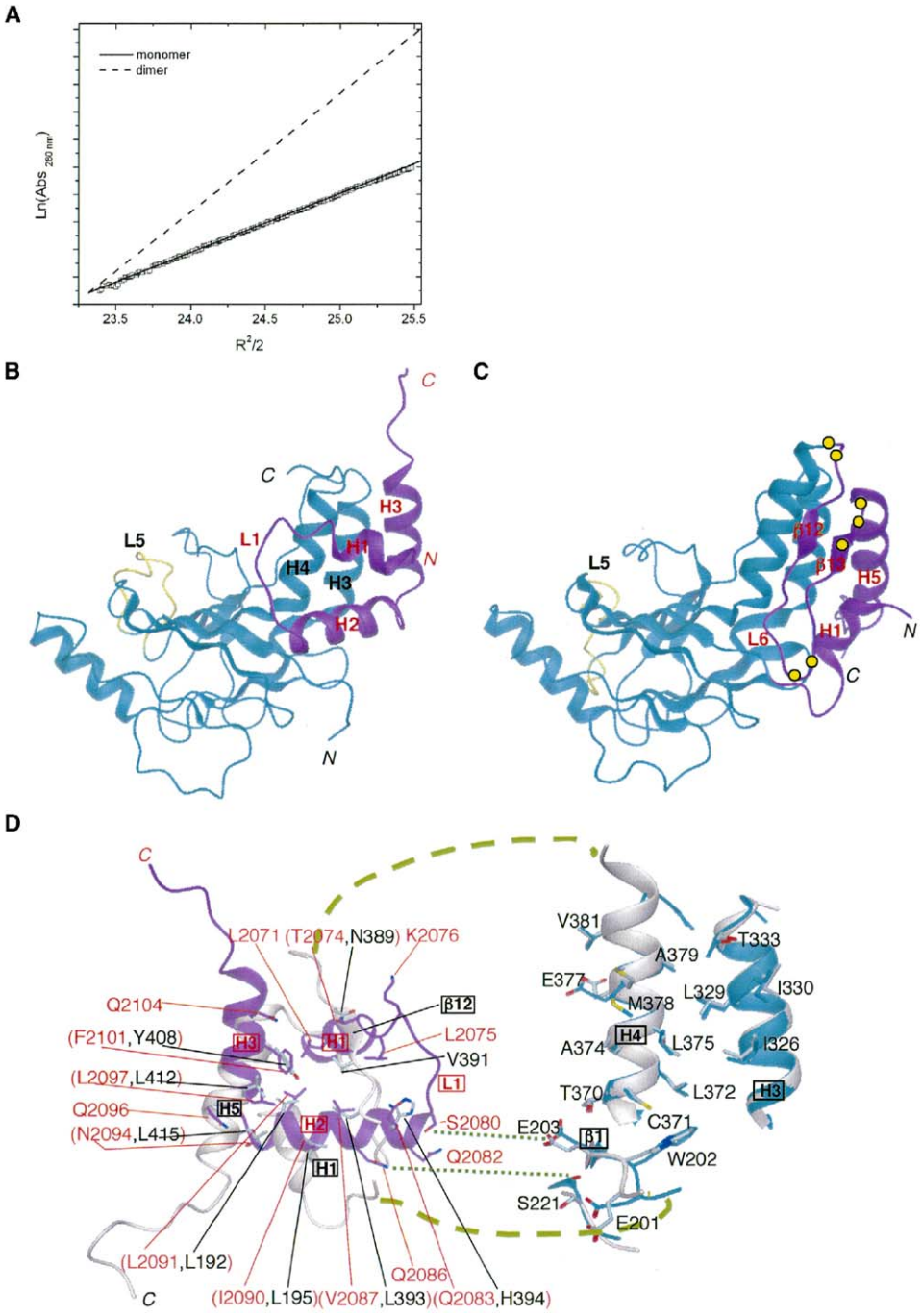

Figure 1. Structural Basis of the IRF-3/IBiD Interaction

(A) Sedimentation equilibrium analysis of the IRF-3/IBiD complex. The experimental data points are open squares.

(B) Crystal structure of the IRF-3/IBiD complex. The IRF-3 is in cyan, and the IBiD is in purple.

(C) Crystal structure of latent IRF-3. The IAD of IRF-3 is colored cyan. The N- and C-terminal autoinhibitory structures are colored purple. The locations of the putative phosphorylation sites that are phosphorylated upon virus infection are indicated by yellow dots.

(D) Comparison of the interface of the IRF-3/IBiD complex (IRF-3 is colored cyan, and the IBiD is colored purple) and the interface buried by the autoinhibitory elements in the latent IRF-3 structure (colored gray). The interaction surfaces are shown side by side by separating the two interacting surfaces. The IRF-3 structure/residues are labeled in black. The IBiD structure/residues are labeled in red. The side chains that are superimposible in space between the IBiD and the autoinhibitory structures of IRF-3 are labeled side by side within parentheses. Hydrogen bond interactions are shown by green dotted lines.

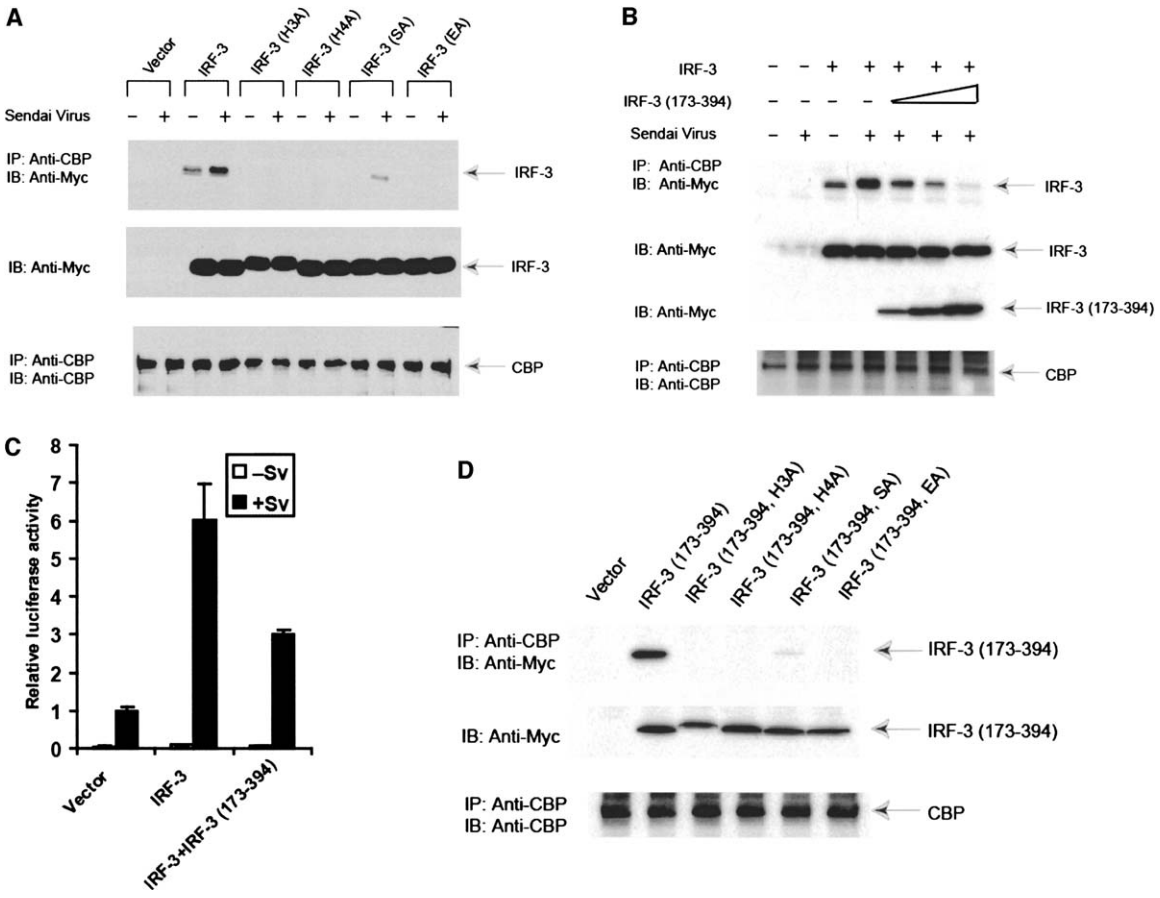

Figure 2. Assays of IRF-3 Interaction with CBP

(A) Interactions of full-length wild-type or mutant IRF-3 with endogenous CBP, as assessed by coimmunoprecipitation analyses in untreated or Sendai virus-infected cells. The mutations generated in each of the mutants are as follows: H3A: Leu322, Pro324, Ile326, Val327, Leu329, and Ile330 replaced by alanine; H4A: Cys371, Leu375, and Met378 replaced by alanine; SA: Ser221 replaced by alanine; EA: Glu201 and Glu203 replaced by alanine.

(B) IRF-3(173-394) interferes with the interaction of wild-type IRF-3 with endogenous CBP. Myc- tagged IRF-3 was coexpressed with increasing levels of myc-tagged IRF-3(173-394) in cells that were subsequently either untreated or infected with Sendai virus. Cell lysates were subjected to immunoprecipitation followed by Western blotting, as indicated.

(C) Effect of IRF-3(173-394) on virus-induced transcription activity of IRF-3. HeLa cells were transfected with the p31x3 reporter plasmid and expression plasmids as indicated, and cells were either untreated or infected with Sendai virus. Luciferases activities were normalized to the expression of a cotransfected β-galactosidase plasmid. The error bars represent standard deviations of duplicate values in a representative experiment.

(D) Mutants of IRF-3(173-394) showed a similar interaction with CBP as the mutants of full-length IRF-3 shown in (A). Experiments were done as in (A).

H3A and H4A mutants contained mutations of the hydrophobic residues in the H3 and H4 helices, respectively, of IRF-3 and were designed to disrupt the hydrophobic interaction with CBP. The SA and EA mutants of IRF-3 were designed to disrupt the polar contacts with CBP, whereas the SA mutant had Ser221 mutated to alanine, and the EA mutant had both Glu201 and Glu203 mutated to alanine. While Myc-tagged, wild-type IRF-3 exhibited some interaction with CBP, which was substantially enhanced by viral infection, the mutants, with the exception of IRF-3(SA), did not detectably interact with CBP in the presence or absence of virus infection. The IRF-3(SA) mutant showed a low-level interaction with CBP in the presence of virus, but no detectable interaction in the absence of virus. These results are consistent with the structure and support that the hydrophobic contacts mediated by the H3 and H4 helices, and the polar contacts mediated by Ser221 and Glu203 of IRF-3, are involved in the interaction of activated IRF-3 with CBP in vivo. The reported substantial decrease in the transactivation activity of IRF-3 resulting from mutations in the H3 and H4 helices (Qin et al., 2003) may therefore be caused by disruption of the interaction between IRF-3 and CBP/p300. To further verify that IRF-3(173-394) used in the structural study faithfully mimics the interaction of full-length IRF-3 with CBP, we performed a competition experiment to assess whether IRF-3(173-394) can compete with Sendai virus-activated, full-length IRF-3 for CBP interaction. As shown in Figure 2B, increasing amounts of IRF-3(173-394) de-

creased the virus-induced association of full-length IRF-3 with endogenous CBP, strongly suggesting that IRF-3(173-394) exhibits the same mode of binding to endogenous CBP as activated full-length IRF-3. Since IRF-3(173-394) cannot bind to the promoter DNA due to the absence of its DNA binding domain, its interaction with CBP does not confer transcription activity (data not shown) and should allow for competitive interference with IRF-3-driven transcription through CBP/p300. Accordingly, coexpression of IRF-3(173-394) decreased the virus-induced transcription activity of IRF-3 from an IRF-3 binding promoter (Figure 2C), demonstrating that IRF-3(173-394) functionally competes with activated IRF-3 for CBP interaction. Finally, the effects of subunit interface mutations on the interaction between IRF-3(173-394) and CBP were tested (Figure 2D). The same mutations were generated in IRF-3(173-394) as in full-length IRF-3 (Figure 2A); however, as the inhibitory domain was removed in this construct, no viral activation was required for the interaction of IRF-3(173-394). Coimmunoprecipitation experiments showed that IRF-3(173-394) interacted well with endogenous CBP, and that this interaction was abolished by the interface mutations. As with full-size IRF-3(SA) following viral activation (Figure 2A), IRF-3(173-394, SA) showed a low-level interaction with CBP (Figure 2D). All of these functional studies indicate that the structure of the IRF-3/IBiD complex is physiologically relevant.

There is a remarkable similarity between the interface of the IRF-3/IBiD complex and the interface buried by the autoinhibitory elements in latent IRF-3. This results from a similar spatial display of the interacting side chains in the IBiD and the IRF-3 autoinhibitory elements, despite their distinct secondary structural arrangements (Figure 1D, left). Specifically, T2074 in the H1 helix of the IBiD occupies the same space as N389 in the autoinhibitory structure; Q2083, V2087, I2090, L2091, and N2094 in the H2 helix of the IBiD occupy the same space as H394, L393, L195, L192, and L415, respectively, in the autoinhibitory structure; L2097 and F2101 in the H3 helix of the IBiD occupy the same space as L412 and Y408, respectively, in the autoinhibitory structure. In addition to the above-mentioned pairs of matching residues, L2071 in the IBiD and V391 in the autoinhibitory structure occupy a distinct, nonoverlapping space, suggesting that a minor structural rearrangement on the complementary interface of IRF-3 is required in the transition from the autoinhibited to the IBiD bound state. Indeed, the side chain of M378 in the H4 helix of IRF-3 needs to undergo a rotameric rearrangement to form a complex with the IBiD (Figure 1D, right).

Complex Formation Requires Conformational Changes in IRF-3

The mutually exclusive nature of the IRF-3 autoinhibitory conformation and the IRF-3/IBiD interaction suggests that the autoinhibitory structures of IRF-3 need to be displaced upon activation. Upon virus infection, the IKK-related kinases, IKKε and/or TBK1, activate latent IRF-3 through phosphorylation of defined Ser/Thr residues within the C-terminal autoinhibitory elements (Fitzgerald et al., 2003; Sharma et al., 2003). The crystal structure of latent IRF-3 revealed that these phosphorylation sites are partially buried in a hydrophobic environment (Figure 1C) (Qin et al., 2003). A plausible activation mechanism, consistent with the structures, is that the repulsive force between the phosphorylated residues and their hydrophobic environment leads to unfolding of the autoinhibitory elements and consequent exposure of the H3 and H4 helices for interaction with the IBiD. The autoinhibitory elements of IRF-3 are not observed in the IRF-3/IBiD complex, due to exclusion of the C-terminal autoinhibitory elements in the expression construct, and the structural disordering of the N-terminal autoinhibitory element.

The L5 loop of IRF-3 in complex with the IBiD assumes a different structural arrangement when compared to that in the autoinhibited IRF-3 (compare Figures 1B and 1C). Although a definitive function of the L5 loop has not been assigned, mutation of the basic residues K360 and R361 within the loop disables the virus-induced IRF-3 oligomerization and transcriptional activation, suggesting that the L5 loop is important for activation (Qin et al., 2003). It is not obvious whether the observed structural change of the L5 loop has functional implication since the L5 loop also forms part of the crystal packing contacts in the IRF-3/IBiD complex.

Complex Formation Requires Conformational Changes in the IBiD

The structure of the uncomplexed IBiD has been investigated by NMR. In one study, the free IBiD forms a small globular domain with three interacting helices (Lin et al., 2001a). However, another study suggested that the free IBiD contains a helical secondary structure, but no fixed tertiary structure, characteristic of a molten globule (Demarest et al., 2004). Thus, the reported structure of the free IBiD, which is used for comparison here, may represent the more stable form among the many possible conformations that can exist in solution.

The IBiD in the IRF-3/IBiD complex has a different conformation when compared to the uncomplexed IBiD structure (Figure 3). The H2 helix in the IRF-3/IBiD complex is longer, as a consequence of a disorder-to-order transition of a glutamine-rich segment from residue 2079 to residue 2085 upon complex formation. The ordering of this region correlates with its direct contact with IRF-3. There is also a significant change in the relative positions of the H1 and H2 helices. When viewed through the plane formed by the H2 and H3 helices, the H1 helix in the IRF-3/IBiD complex points toward the opposite side of the plane as compared to that in the uncomplexed structure (Figure 3, right). These structural rearrangements of the IBiD make available a cluster of the above-mentioned hydrophobic side chains that are important for interaction with IRF-3 but are otherwise buried in an intramolecular hydrophobic core in the uncomplexed structure.

Two Distinct Conformations of the IBiD Induced by Different Transcriptional Partners

As mentioned, the IBiD can interact with diverse transcriptional partners with no apparent sequence or structural homology. In addition to the IRF-3/IBiD complex structure described here, an NMR structure of a

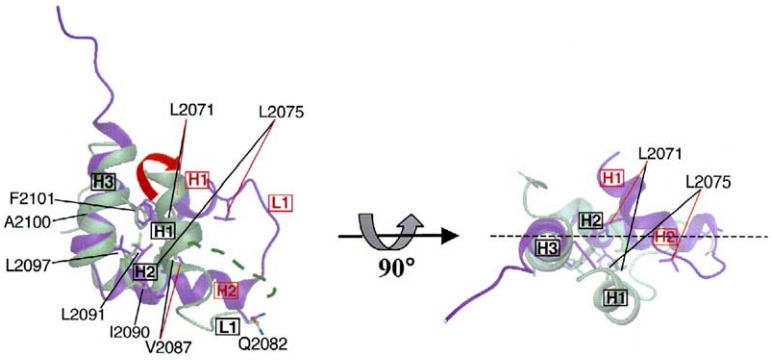

Figure 3. The IBiD Undergoes Conformational Changes upon IRF-3 Interaction

The structure of the IBiD in the IRF-3/IBiD complex (purple ribbon) and the NMR structure of the uncomplexed IBiD (green ribbon) are superimposed, thereby aligning the H3 helices. The left and right views are related by an approximately 90° rotation about a horizontal axis. The uncomplexed structure is labeled in black. The parts of the complexed structure that have different conformations as compared to the uncomplexed structure are indicated in red. The dotted line indicates the plane formed by the H3 and H2 helices.

complex between the IBiD and the steroid hormone receptor coactivator ACTR has been reported (Demarest et al., 2002). Comparison of both the IBiD complex structures demonstrates different IBiD conformations dictated by the interacting transcriptional partner. Unlike the contacts of the IBiD with IRF-3 through a planar interface, the IBiD forms a V-shaped pocket to embrace ACTR, with the H3 helix lining up one side of the pocket and the H1-L1-H2 structure capping the other side (Figure 4). There is a marked difference in the relative position of the N and C termini between the two drastically different conformations of the IBiD. Since the IBiD is an internal segment of CBP, these observations suggest that the differences in the IBiD structures, depending upon the interaction transcriptional partner, may propagate into global differences in CBP/p300 structures in the two different complexes.

Despite the distinct mode of contacts in the two IBiD complexes, the same set of hydrophobic residues mentioned above is used by the IBiD for interaction. Three factors appear to facilitate the adaptability of the IBiD in macromolecular recognition. First, the flexibility of the L1 loop in the IBiD allows the H1 helices in the two different complexes to swing in different directions, pivoting about the flexible L1 loop, while keeping the relative angle between the H2 and H3 helices largely unchanged. Second, the polyglutamine sequences of the IBiD in the two complexes can be induced to form different structures upon complex formation. In the IRF-3/IBiD complex, the polyglutamine sequence forms an extended H2 helix (Figure 4, left), and most of the glutamine side chains participate in van der Waals contacts with IRF-3, with the exception of Gln2086, which forms an H bond with the side chain of Ser221 of IRF-3. In the ACTR/IBiD complex, the polyglutamine sequence forms a coil-like structure, with most of the glutamine side chains projecting into the solvent without specific interactions with ACTR (Figure 4, right) (Demarest et al., 2002). Finally, distinct sets of polar residues within the IBiD are employed as specificity determinants in the two complexes. In the ACTR/IBiD complex, Arg2105, Asn2094, Ser2079, and Lys2108 of the IBiD participate in hydrophilic contacts with ACTR (Demarest et al., 2002). In the IRF-3/IBiD complex, none of these IBiD residues are involved in the hydrophilic contacts. Instead, Ser2080 and Gln2086 mediate hydrophilic contacts with IRF-3 on the outskirts of the IRF-3/IBiD complex. The structural comparison suggests the possibility that the IBiD may function as an allosteric control site in CBP/p300, where different transcriptional allosteric effectors not only compete to bind, but also induce distinct conformational changes in CBP/p300. The two distinct conformations of CBP/p300 may then recognize different combinations of additional transcriptional regulators, or may have different acetyltransferase activities, thus differentially defining the role of CBP/p300 in transcriptional regulation.

Discussion

The crystal structure of the IRF-3/IBiD complex reported here strongly supports the previously proposed autoinhibitory mechanism in latent IRF-3 (Lin et al., 1998, 1999; Qin et al., 2003; Wathelet et al., 1998), since

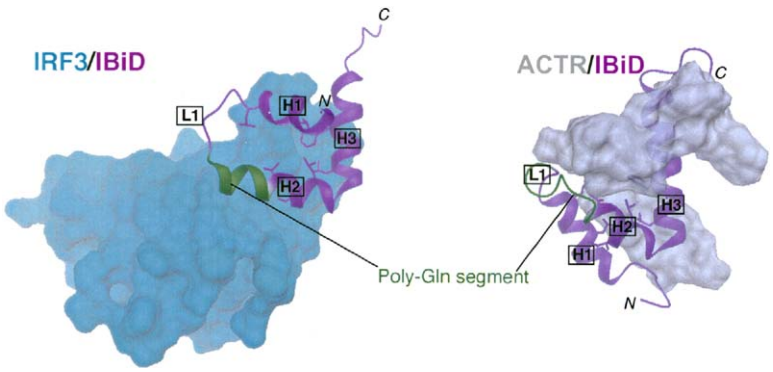

Figure 4. Different Transcriptional Partners Induce Distinct IBiD Conformations

Left: the crystal structure of the IRF-3/IBiD complex. The IRF-3 IAD is shown in surface representation. The IBiD is shown in ribbon representation. Right: the NMR structure of the ACTR/IBiD complex. The ACTR is shown in surface representation. The IBiD is shown in ribbon representation. The H2 and H3 helices of the IBiD in the two complexes are in approximately the same relative position in the view presented.

the IBiD occupies the same binding site as the N- and C-terminal structures of IRF-3 in the latent IRF-3 structure. The structure demonstrates that these autoinhibitory elements have to be displaced during activation to allow CBP to interact with IRF-3, presumably through virus-induced phosphorylation and unfolding of the C-terminal segment. The structure also reveals that oligomerization of IRF-3 is not required for CBP interaction, since both the crystal structure and analytical ultracentrifugation reveal a 1:1 complex between IRF-3 and CBP. It should be noted that this finding does not contradict the current paradigm of IRF-3 activation, in which virus-induced phosphorylation of IRF-3 leads to its dimerization, nuclear translocation, and interaction with CBP/p300. Rather, the result suggests that a distinct structural domain not present in the crystal structure, probably the C-terminal tail, is responsible for oligomerization. Consistent with this notion, a phosphomimetic form of IRF-3, IRF-3(S396/398D), in which both Ser396 and Ser398 phosphorylation sites within the C-terminal tail were mutated to aspartic acids, forms a complex with the IBiD, and this complex has a strong propensity to oligomerize (data not shown). This difference with the behavior of unphosphorylated IRF-3, merely due to pseudophosphorylation of the two serines, indicates that the phosphorylated C-terminal sequence of IRF-3 plays a primary role in IRF-3 oligomerization, potentially by bridging subunit-subunit contacts. Although the structure of the active, oligomeric state of IRF-3 in complex with CBP remains to be elucidated, further conformational changes of the IBiD in the oligomeric form of IRF-3 are not anticipated, as the structure is supported by mutational analysis in the virus infection assay, which represents the interaction of activated wild-type IRF-3 with CBP.

This work also reveals the unique features on IRF-3 that are responsible for its interaction with CBP/p300. The interactions are mediated by hydrophobic contacts via the H3 and H4 helices as well as hydrophilic contacts through Glu203 and Ser221. These interacting residues on IRF-3 are only partially conserved in other IRF family members, suggesting that other IRFs employ alternative structural strategies for interaction or do not interact with CBP/p300. For example, it was demonstrated that the interaction between IRF-7 and CBP/p300 requires multiple regions of the CBP/p300 (Yang et al., 2003). Consistently, Glu203 and Ser221 as well as a subset of the hydrophobic residues on the H3 and H4 helices of IRF-3 are not conserved in IRF-7, making it unlikely for the IBiD alone to interact with IRF-7. In this regard, it is interesting to speculate that there may be significant differences in the way CBP/p300 interacts with the homodimeric IRF-3 versus the heterodimeric IRF-3/IRF-7 and IRF-3/IRF-5 (Barnes et al., 2001; Wathelet et al., 1998). The homodimeric IRF-3 may interact with two molecules of CBP/p300, each at the IBiD, and induce a symmetrical conformational change in CBP/p300. The heterodimeric IRF species may still interact with two CBP/p300 molecules, but with different structural consequences on CBP/p300 since only IRF-3 can interact strongly with the IBiD. These dimeric species of IRF have been shown to activate transcription of the type I IFN genes, but with different target preferences (Barnes et al., 2001, 2004; Lin et al., 2000; Marie et al., 1998; Sato et al., 2000). Whether the differences in their interactions with CBP/p300 play a role in target gene selection remains to be investigated.

We previously proposed that the IRF family members use a similar structural strategy for signaling as the Smad family of proteins (Qin et al., 2003), which are signal transducers and transcription factors of the transforming growth factor β (TGF-β) pathway. The two protein families share a common structural fold and display similar surface electrostatic potential distribution. Similar to IRF-3, the receptor-activated Smads (R-Smads) oligomerize upon activation and enter the nucleus to regulate transcription of target genes. The identification of the hydrophobic surface on IRF-3 as the site of CBP interaction strongly supports this proposal, as the corresponding hydrophobic surface on Smad2/3 plays a versatile role, sequentially interacting with a number of proteins along the signaling pathway. At the cell membrane, Smad2/3 interacts with the membrane-anchored protein SARA to allow efficient receptor phosphorylation (Qin et al., 2002; Tsukazaki et al., 1998; Wu et al., 2000). During nuclear transit, it interacts with the nucleoporins CAN/Nup214 and Nup153 (Xu et al., 2002). In the nucleus, it interacts with CBP/p300 or the transcriptional repressor Ski in a mutually exclusive manner (Luo et al., 1999; Qin et al., 2002; Wu et al., 2001). Further studies will reveal whether the hydrophobic surface on IRF-3 has other interaction roles besides its intramolecular association to confer latency and its association with CBP/p300.

Allosteric control of coactivator function may be a general mechanism for regulating transcription. It has been observed, by using electron microscopy and three-dimensional reconstruction, that the multisubunit coactivator complex CRSP assumes different conformations upon binding different transcription factors (Taatjes et al., 2002, 2004). Each transcription factor interacts with a distinct subunit of the CRSP complex to induce a subunit conformational change that propagates to the entire coactivator molecule. In comparison, CBP/p300 undergoes activator-dependent conformational changes via a single site, the IBiD, which forms different structures upon binding different activators. Despite the different mechanisms, an activator-induced conformational change of coactivators is likely to play a key role in transcriptional regulation. A coactivator's conformation may define the repertoire of transcription factors that it binds and hence the genes that it regulates. A conformational change may also control the coactivator's enzymatic function and/or its communication with the polymerase. Further studies will be necessary to address these possibilities.

In conclusion, the studies described here reveal the structural basis of IRF-3 interaction with the transcriptional coactivator CBP/p300 and shed light on the mechanism of IRF-3 activation. The observation that the IBiD of CBP/p300 can assume drastically distinct conformations depending on the identity of the interacting transcriptional partner implies an allosteric model in CBP/p300 function, where binding of a comodulator to CBP/p300 may influence the overall conformation of CBP/p300 and its function in transcription. This mechanism

provides another level of regulation in the control of gene expression.

Experimental Procedures

Protein Expression, Purification, and Crystallization

The sequences encoding the IAD of IRF-3 (residues 173-394) and the IBiD of CBP (residues 2067–2112) were subcloned into pGEX-6P-1 and pET-28a, respectively, and coexpressed in *E. coli*. The complex was extracted by glutathione Sepharose and released by PreScission Protease to remove the GST moiety (Amersham). The complex was further purified on a DEAE column equilibrated with 20 mM Tris (pH 7.4), 10 mM NaCl, 0.1 mM EDTA, and 1 mM DTT and was eluted by a NaCl gradient from 10 mM to 300 mM. The purified complex was concentrated to 12 mg/ml. Crystals were obtained by the hanging drop vapor diffusion technique with well solution containing 0.2 M ammonium acetate, 0.15 M Mg acetate, 5% (v/v) PEG 4000, and 50 mM Na HEPES (pH 7.0).

Structure Determination

The IRF-3/IBiD crystals were transferred into a cryosolvent containing 75% of the well solution and 25% glycerol and were flash frozen in liquid nitrogen. Data were collected at beam line 5.0.1 of the Advanced Light Source at Berkeley Lab (Berkeley, California). The IRF-3/IBiD complex structure was determined by molecular replacement by using the IAD portion of the autoinhibited IRF-3 crystal structure as the search model (Qin et al., 2003). Solutions for the two copies of IRF-3 in the asymmetric unit were located with the program MOLREP in CCP4 (CCP4, 1994). Calculation of the electron density map by using the IRF-3 model revealed additional density corresponding to that of the IBiD and allowed for manual building of the IBiD structure into the density. The structure of the complex was refined by using the conjugated gradient and simulated annealing protocols in CNS (Brunger et al., 1998). Model rebuilding was performed with O (Jones et al., 1991). The final structure contains the following residues: chains A and B (IRF-3), residues 196–386; chains C and D (the IBiD), residues 2065–2111.

Analytical Ultracentrifugation

Sedimentation equilibrium and velocity experiments were performed as a function of loading concentration, at 19.7°C, in a buffer containing 20 mM HEPES, 0.1 mM EDTA, and 100 mM NaCl at pH 7.3. Density was measured to be 1.00445 in an Anton Paar DMA 5000 at 19.7°C. Both techniques revealed concentration independence and the presence of a 1:1 monomeric IRF-3/CBP complex with a small amount of irreversible dimer (7.6%). Six sedimentation equilibrium data sets (4.4–10.6 μM at 24 K) were analyzed with Winnonl and were best fit to a single species model (MW = 31,591 ± 661, rms = 0.00578) (Johnson et al., 1981). Three sedimentation velocity data sets (5.3–17.2 μM at 42 K) were analyzed with Sedanal (Sontag et al., 2004; Stafford and Sherwood, 2004) and were also best fit to a single species model (MW = 30,926, S = 2.470, rms = 0.00426). To demonstrate this, one data set was plotted as LnC versus $r^2/2$ and compared to the expected line for a monomer and a dimer (Figure 1A). Thus, the IRF-3/CBP complex is a monomer under these conditions and over this concentration range.

Immunoprecipitation and Western Blot Analysis

Expression plasmids for Myc-tagged IRF-3, or IRF-3(173-394) or their mutants, were made by using PCR-based mutagenesis and amplification of the needed DNA fragments that were then inserted into XF1-myc vector (Qin et al., 2003). Details of the mutagenesis and plasmid constructions will be provided upon request. 293T cells were transfected with expression plasmids encoding Myc-tagged, full-length wild-type or mutated IRF-3 or IRF-3(173-394) by using Lipofectamine Plus (Invitrogen). At 24 hr after transfection, cells were infected with Sendai virus (80 HA units/ml) for 12 hr. Whole-cell lysates were prepared in MLB buffer (20 mM Tris-HCl [pH 7.5], 200 mM NaCl, 1% [v/v] NP-40, and complete protease inhibitors [Roche]) and were immunoprecipitated with 1 μg anti-CBP A-22 (Santa Cruz) and protein A-Sepharose 4B (Amersham-Pharmacia). Immunoprecipitated proteins were separated on SDS-PAGE. Western blotting was carried out with anti-Myc 9E10 (Covance) or anti-CBP A-22. Bands were visualized by using ECL reagents (Amersham-Pharmacia).

For transcription reporter assays, HeLa cells were transiently transfected with the P31x3 reporter plasmid and β-galactosidase expression plasmid, as well as the IRF-3 expression plasmid(s), as indicated (Figure 2C). All transfected DNA amounts were kept constant by adding empty expression vector as needed. Infection with Sendai virus (100 HA units/ml) was done at 24 hr after transfection for 20 hr. Luciferase assays were carried out and normalized as described (Qin et al., 2003).

Supplemental Data

Supplemental data including the complete analytical ultracentrifugation analysis are available at http://www.structure.org/cgi/content/full/13/9/1269/DC1/.

Acknowledgments

We thank the staff members of Advanced Light Source for assistance with the data collection of the IRF-3/CBP complex. This work was supported by grants from the National Institutes of Health to K.L. and R.D.

Received: January 5, 2005
Revised: May 6, 2005
Accepted: June 10, 2005
Published: September 13, 2005

References

Barnes, B.J., Moore, P.A., and Pitha, P.M. (2001). Virus-specific activation of a novel interferon regulatory factor, IRF-5, results in the induction of distinct interferon α genes. J. Biol. Chem. *276*, 23382–23390.

Barnes, B., Lubyova, B., and Pitha, P.M. (2002). On the role of IRF in host defense. J. Interferon Cytokine Res. *22*, 59–71.

Barnes, B.J., Richards, J., Mancl, M.E., Hanash, S., Beretta, L., and Pitha, P.M. (2004). Global and distinct targets of IRF-5 and IRF-7 during innate response to viral infection. J. Biol. Chem. *279*, 45194–45207.

Blobel, G.A. (2002). CBP and p300: versatile coregulators with important roles in hematopoietic gene expression. J. Leukoc. Biol. *71*, 545–556.

Brunger, A.T., Adams, P.D., Clore, G.M., DeLano, W.L., Gros, P., Grosse-Kunstleve, R.W., Jiang, J.S., Kuszewski, J., Nilges, M., Pannu, N.S., et al. (1998). Crystallography & NMR system: a new software suite for macromolecular structure determination. Acta Crystallogr. D Biol. Crystallogr. *54*, 905–921.

CCP4 (Collaborative Computational Project, Number 4)(1994). The CCP4 suite: programs for protein crystallography. Acta Crystallogr. D Biol. Crystallogr. *50*, 760–763.

Chan, H.M., and La Thangue, N.B. (2001). p300/CBP proteins: HATs for transcriptional bridges and scaffolds. J. Cell Sci. *114*, 2363–2373.

Demarest, S.J., Martinez-Yamout, M., Chung, J., Chen, H., Xu, W., Dyson, H.J., Evans, R.M., and Wright, P.E. (2002). Mutual synergistic folding in recruitment of CBP/p300 by p160 nuclear receptor coactivators. Nature *415*, 549–553.

Demarest, S.J., Deechongkit, S., Dyson, H.J., Evans, R.M., and Wright, P.E. (2004). Packing, specificity, and mutability at the binding interface between the p160 coactivator and CREB-binding protein. Protein Sci. *13*, 203–210.

Fitzgerald, K.A., McWhirter, S.M., Faia, K.L., Rowe, D.C., Latz, E., Golenbock, D.T., Coyle, A.J., Liao, S.M., and Maniatis, T. (2003). IKKε and TBK1 are essential components of the IRF3 signaling pathway. Nat. Immunol. *4*, 491–496.

Goodman, R.H., and Smolik, S. (2000). CBP/p300 in cell growth, transformation, and development. Genes Dev. *14*, 1553–1577.

Hiscott, J., Pitha, P., Genin, P., Nguyen, H., Heylbroeck, C., Mamane, Y., Algarte, M., and Lin, R. (1999). Triggering the interferon

response: the role of IRF-3 transcription factor. J. Interferon Cytokine Res. *19*, 1–13.

Janknecht, R., and Hunter, T. (1996). Versatile molecular glue. Transcriptional control. Curr. Biol. *6*, 951–954.

Johnson, M.L., Correia, J.J., Yphantis, D.A., and Halvorson, H.R. (1981). Analysis of data from the analytical ultracentrifuge by nonlinear least-squares techniques. Biophys. J. *36*, 575–588.

Jones, A.T., Zou, J.-Y., Cowan, S.W., and Kjeldgaard, M. (1991). Improved methods for building proteins models in electron-density maps and the location of errors in these models. Acta Crystallogr. *A47*, 110–119.

Lin, R., Heylbroeck, C., Pitha, P.M., and Hiscott, J. (1998). Virus-dependent phosphorylation of the IRF-3 transcription factor regulates nuclear translocation, transactivation potential, and proteasome-mediated degradation. Mol. Cell. Biol. *18*, 2986–2996.

Lin, R., Mamane, Y., and Hiscott, J. (1999). Structural and functional analysis of interferon regulatory factor 3: localization of the transactivation and autoinhibitory domains. Mol. Cell. Biol. *19*, 2465–2474.

Lin, R., Genin, P., Mamane, Y., and Hiscott, J. (2000). Selective DNA binding and association with the CREB binding protein coactivator contribute to differential activation of α/β interferon genes by interferon regulatory factors 3 and 7. Mol. Cell. Biol. *20*, 6342–6353.

Lin, C.H., Hare, B.J., Wagner, G., Harrison, S.C., Maniatis, T., and Fraenkel, E. (2001a). A small domain of CBP/p300 binds diverse proteins: solution structure and functional studies. Mol. Cell *8*, 581–590.

Lin, R., Genin, P., Mamane, Y., Sgarbanti, M., Battistini, A., Harrington, W.J., Jr., Barber, G.N., and Hiscott, J. (2001b). HHV-8 encoded vIRF-1 represses the interferon antiviral response by blocking IRF-3 recruitment of the CBP/p300 coactivators. Oncogene *20*, 800–811.

Livengood, J.A., Scoggin, K.E., Van Orden, K., McBryant, S.J., Edayathumangalam, R.S., Laybourn, P.J., and Nyborg, J.K. (2002). p53 Transcriptional activity is mediated through the SRC1-interacting domain of CBP/p300. J. Biol. Chem. *277*, 9054–9061.

Luo, K., Stroschein, S.L., Wang, W., Chen, D., Martens, E., Zhou, S., and Zhou, Q. (1999). The Ski oncoprotein interacts with the Smad proteins to repress TGFβ signaling. Genes Dev. *13*, 196–206.

Maniatis, T., Falvo, J.V., Kim, T.H., Kim, T.K., Lin, C.H., Parekh, B.S., and Wathelet, M.G. (1998). Structure and function of the interferon-β enhanceosome. Cold Spring Harb. Symp. Quant. Biol. *63*, 609–620.

Marie, I., Durbin, J.E., and Levy, D.E. (1998). Differential viral induction of distinct interferon-α genes by positive feedback through interferon regulatory factor-7. EMBO J. *17*, 6660–6669.

Matsuda, S., Harries, J.C., Viskaduraki, M., Troke, P.J., Kindle, K.B., Ryan, C., and Heery, D.M. (2004). A conserved α-helical motif mediates the binding of diverse nuclear proteins to the SRC1 interaction domain of CBP. J. Biol. Chem. *279*, 14055–14064.

Parekh, B.S., and Maniatis, T. (1999). Virus infection leads to localized hyperacetylation of histones H3 and H4 at the IFN-β promoter. Mol. Cell *3*, 125–129.

Qin, B.Y., Lam, S.S., Correia, J.J., and Lin, K. (2002). Smad3 allostery links TGF-β receptor kinase activation to transcriptional control. Genes Dev. *16*, 1950–1963.

Qin, B.Y., Liu, C., Lam, S.S., Srinath, H., Delston, R., Correia, J.J., Derynck, R., and Lin, K. (2003). Crystal structure of IRF-3 reveals mechanism of autoinhibition and virus-induced phosphoactivation. Nat. Struct. Biol. *10*, 913–921.

Sato, M., Suemori, H., Hata, N., Asagiri, M., Ogasawara, K., Nakao, K., Nakaya, T., Katsuki, M., Noguchi, S., Tanaka, N., et al. (2000). Distinct and essential roles of transcription factors IRF-3 and IRF-7 in response to viruses for IFN-α/β gene induction. Immunity *13*, 539–548.

Servant, M.J., Grandvaux, N., and Hiscott, J. (2002). Multiple signaling pathways leading to the activation of interferon regulatory factor 3. Biochem. Pharmacol. *64*, 985–992.

Sharma, S., tenOever, B.R., Grandvaux, N., Zhou, G.P., Lin, R., and Hiscott, J. (2003). Triggering the interferon antiviral response through an IKK-related pathway. Science *300*, 1148–1151.

Sontag, C.A., Stafford, W.F., and Correia, J.J. (2004). A comparison of weight average and direct boundary fitting of sedimentation velocity data for indefinite polymerizing systems. Biophys. Chem. *108*, 215–230.

Stafford, W.F., and Sherwood, P.J. (2004). Analysis of heterologous interacting systems by sedimentation velocity: curve fitting algorithms for estimation of sedimentation coefficients, equilibrium and kinetic constants. Biophys. Chem. *108*, 231–243.

Taatjes, D.J., Naar, A.M., Andel, F., 3rd, Nogales, E., and Tjian, R. (2002). Structure, function, and activator-induced conformations of the CRSP coactivator. Science *295*, 1058–1062.

Taatjes, D.J., Schneider-Poetsch, T., and Tjian, R. (2004). Distinct conformational states of nuclear receptor-bound CRSP-Med complexes. Nat. Struct. Biol. *11*, 664–671.

Takahasi, K., Suzuki, N.N., Horiuchi, M., Mori, M., Suhara, W., Okabe, Y., Fukuhara, Y., Terasawa, H., Akira, S., Fujita, T., et al. (2003). X-ray crystal structure of IRF-3 and its functional implications. Nat. Struct. Biol. *10*, 922–927.

Taniguchi, T., and Takaoka, A. (2002). The interferon-α/β system in antiviral responses: a multimodal machinery of gene regulation by the IRF family of transcription factors. Curr. Opin. Immunol. *14*, 111–116.

Taniguchi, T., Ogasawara, K., Takaoka, A., and Tanaka, N. (2001). IRF family of transcription factors as regulators of host defense. Annu. Rev. Immunol. *19*, 623–655.

Tsukazaki, T., Chiang, T.A., Davison, A.F., Attisano, L., and Wrana, J.L. (1998). SARA, a FYVE domain protein that recruits smad2 to the TGF-β receptor. Cell *95*, 779–791.

Wathelet, M.G., Lin, C.H., Parekh, B.S., Ronco, L.V., Howley, P.M., and Maniatis, T. (1998). Virus infection induces the assembly of coordinately activated transcription factors on the IFN-β enhancer in vivo. Mol. Cell *1*, 507–518.

Weaver, B.K., Kumar, K.P., and Reich, N.C. (1998). Interferon regulatory factor 3 and CREB-binding protein/p300 are subunits of double-stranded RNA-activated transcription factor DRAF1. Mol. Cell. Biol. *18*, 1359–1368.

Wu, G., Chen, Y.-G., Ozdamar, B., Gyuricza, C.A., Chong, P.A., Wrana, J.L., Massague, J., and Shi, Y. (2000). Structural basis of smad2 recognition by the smad anchor for receptor activation. Science *287*, 92–97.

Wu, J.W., Hu, M., Chai, J., Seoane, J., Huse, M., Li, C., Rigotti, D.J., Kyin, S., Muir, T.W., Fairman, R., et al. (2001). Crystal structure of a phosphorylated Smad2. Recognition of phosphoserine by the MH2 domain and insights on Smad function in TGF-β signaling. Mol. Cell *8*, 1277–1289.

Xu, L., Kang, Y., Col, S., and Massague, J. (2002). Smad2 nucleocytoplasmic shuttling by nucleoporins CAN/Nup214 and Nup153 feeds TGFβ signaling complexes in the cytoplasm and nucleus. Mol. Cell *10*, 271–282.

Yang, H., Lin, C.H., Ma, G., Baffi, M.O., and Wathelet, M.G. (2003). Interferon regulatory factor-7 synergizes with other transcription factors through multiple interactions with p300/CBP coactivators. J. Biol. Chem. *278*, 15495–15504.

Yoneyama, M., Suhara, W., Fukuhara, Y., Fukuda, M., Nishida, E., and Fujita, T. (1998). Direct triggering of the type I interferon system by virus infection: activation of a transcription factor complex containing IRF-3 and CBP/p300. EMBO J. *17*, 1087–1095.

Yoneyama, M., Suhara, W., and Fujita, T. (2002). Control of IRF-3 activation by phosphorylation. J. Interferon Cytokine Res. *22*, 73–76.

Accession Numbers

The coordinates and structure factors for the IRF-3/CBP complex have been deposited in the Protein Data Bank under the accession number 1Z0Q.